Fluid Mechanics of Arterial Stenosis: Relationship to the Development of Mural Thrombus

Danny Bluestein,* Lijun Niu,* Richard T. Schoephoerster,* and
Mrinal K. Dewanjee†

*Department of Mechanical Engineering, Florida International University; and †Department of Radiology,
Division of Nuclear Medicine, University of Miami, Miami, FL

Abstract—In this study, we analyzed blood flow through a model stenosis with Reynolds numbers ranging from 300 to 3,600 using both experimental and numerical methods. The jet produced at the throat was turbulent, leading to an axisymmetric region of slowly recirculating flow. For higher Reynolds numbers, this region became more disturbed and its length was reduced. The numerical predictions were confirmed by digital particle image velocimetry and used to describe the fluid dynamics mechanisms relevant to prior measurements of platelet deposition in canine blood flow (R. T. Schoephoerster et al., Atherosclerosis and Thrombosis 12:1806–1813, 1993). Actual deposition onto the wall was dependent on the wall shear stress distribution along the stenosis, increasing in areas of flow recirculation and reattachment. Platelet activation potential was analyzed under laminar and turbulent flow conditions in terms of the cumulative effect of the varying shear and elongational stresses, and the duration platelets are exposed to them along individual platelet paths. The cumulative product of shear rate and exposure time along a platelet path reached a value of 500, half the value needed for platelet activation under constant shear (J. M. Ramstack et al., Journal of Biomechanics 12: 113–125, 1979).

Keywords—Arterial stenosis, Fluid mechanics, Mural thrombus, Platelet deposition.

INTRODUCTION

Mural thrombosis and embolization are frequently associated with arterial coronary stenoses, and play a central role in the development of unstable angina, myocardial infarction, and sudden ischemic death (21). The process of thrombosis may be affected by a series of rheological and fluid dynamic parameters, including high rates of shear, areas of flow stagnation or recirculation, and turbulence (10,15). Transfer of platelets and other clotting factors to the vascular wall is accomplished through diffusive and convective mechanisms. The convection of flow aggregates can be locally enhanced or diminished in arterial stenosis through localized regions of high shear, flow separation, recirculation, and reattachment.

Numerous studies have been performed (25) to determine the flow and pressure characteristics of arterial stenosis. Stein and Sabbah (21) have correlated turbulence with thrombus formation on artificial surfaces. Near wall excesses of platelets in tube flow have been reported to be dependent, among other factors, on flow conditions (e.g., wall shear rate) and tube diameter (1,23). Direct correlations of local fluid dynamic events with platelet aggregation in vortices and adhesion onto surfaces were obtained in low Reynolds number flow through an abrupt expansion (13,14). Actual deposition of platelets onto artificial surfaces tended to increase with increasing shear due to increased collision frequency and mass transfer (4,17). Eckstein and Belgacem (8) modeled the near-wall excesses platelet concentration, taking into account drift and diffusion terms.

Studies of blood flow through a stenosis using tunica media as a model for damaged vessel wall (2,16), or collagen-coated shunts, have shown increased platelet adhesion on the apex of a stenosis wherein fluid shear forces and shear-rate dependent diffusion are maximum. However, other studies did not show an increase in deposition with increased shear for noncollagen-coated shunts (9), a decrease in platelet deposition onto a Lexan surface in the throat region of the stenosis supplemented by an increase in the downstream recirculation region (20), or a decreased deposition of plate-

lets with increased flow rate through a hollow fiber hemodialyzer with canine and human blood (7). It is likely that these contrary findings can be attributed mainly to differences in surface-platelet adhesive forces at the wall.

Several works studied the combined effect of shear and exposure time on platelet activation. For canine blood flow in cylindrical tubes, Ramstack et al. (19) showed that platelet stimulation is a nonlinear phenomenon, wherein a large stress for a short duration can cause significant platelet stimulation, whereas the same stress for an additional increment of time can cause relatively less stimulation. They also analyzed results of previous research, and showed that the percentage of platelet trauma as a function of the product of bulk shear rate and residence time follows an exponential growth curve. Phenomenological studies of platelet response (11,12) led to a depiction of a locus of incipient shear-related platelet serotonin release on a shear stress-exposure time plane. Sutera et al. (22) showed that pulsed exposure resulted in more platelet aggregation than continuous exposure for the same total exposure time to stress, indicating shear and velocity gradients as enhancing platelet activation. The previously described studies, however, were conducted in devices that produced constant shear stress/shear rate levels, with only the exposure time, that was much longer than physiological time scales, varying. More physiological time scales were used by Colantuoni et al. (5), who showed serotonin release for short exposure times of 1 to 5 msec at shear stresses >7,000 dyne/cm². Little previous work has been reported on the effects of elongational stresses on platelet activation; yet, when a platelet flows through a stenosis, the convective acceleration produces such stresses. Purvis and Giorgio (18) showed that platelets exposed to elongational stresses tend to form large aggregates and may induce platelet activation even at low shear levels. Thus, application of the platelet activation criteria established by most previous in vitro research efforts to more realistic physiological conditions is questionable. The devices used to induce the shear stresses (e.g., cone and plate viscometers, capillary tube viscometers, etc.) were able to produce physiological shear rates. However, in most of the cases, constant shear rates were applied, and for durations much longer than physiological. In very few cases, varying shear rates were applied, but lagged far behind physiological.

Although previous numerical studies have provided useful information, in many cases important limitations and restrictions were applied (e.g., the use of Reynolds numbers that are much lower than those found in pathological conditions in the cardiovascular system, the violation of boundary conditions due to the use of a too short computational domain, and other restrictions that stem from past computational capabilities). Whereas many of these works studied the wall shear stresses, almost none have tried to estimate the shear stresses within the flow domain, wherein most of the platelet activation process takes place. Although turbulence was shown to be a crucial agent in thrombus formation and turbulent flow patterns usually arise under stenotic conditions, turbulent numerical stimulations are scarce. When considering a platelet activation process, the platelet is exposed to varying levels of shear stress as it passes through various flow regions. From the point of view of an observer that moves with the platelet (Lagrangian point of view), these stresses will change in time and space even under steady-flow conditions. This indicates that fluid-induced platelet activation should be analyzed in terms of the combined effect of the varying shear stress levels and the duration the platelet is exposed to them. A platelet might not be activated by an instantaneous shear stress level, but eventually it might be activated if it is exposed to this stress level for a longer duration. Thus, time histories of individual platelets should be tracked down within the flow domain to locate the regions where activated platelets might be found and subsequently adhere to the wall.

Experiments in which platelet deposition onto the wall at a stenosis and the associated flow dynamics were measured were not found in the literature. The purpose of the present study was to obtain qualitative and quantitative relations of fluid dynamic parameters under pathological flow conditions, with platelet deposition onto artificial surfaces. Those were obtained in a axisymmetric geometry that models pathologies in the natural human circulation, yet produces well-controlled fluid flow phenomena (i.e., well-defined recirculation zone, etc.). Flow patterns—like areas of flow separation, recirculation, and reattachment—were qualitatively correlated to the platelet deposition. Fluid flow parameters that were quantitatively correlated with platelet deposition included turbulent and wall shear stresses, shear and elongational stresses, and residence times along individual platelets paths within the flow domain. Those were then used to estimate the activation potential of the platelets.

METHODS

Both experimental and numerical methods were used to study steady in vitro flow patterns under laminar and turbulent flow conditions through a streamlined axisymmetric stenosis model geometry (Fig. 1) used by other researchers (6,26). Contraction and
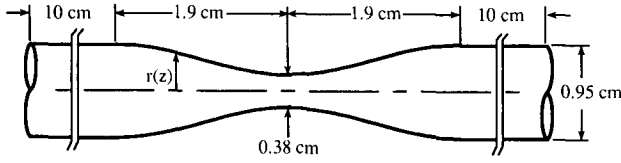
FIGURE 1. Geometry of the streamlined axisymmetric stenosis model used for the numerical simulations as well as the earlier platelet deposition experiments. The contraction and expansion in the flow geometry follow a sinusoidal function, which results in an area reduction of 84%. The DPIV measurements were carried out in a larger scale (10:1) model.

expansion in the flow geometry follow a sinusoidal function of the form:

$$r(z) = 0.47 - 0.14\,[1 + \cos{(\pi z/1.9)}], \qquad (1)$$

where $r(z)$ is the local radius of the tube, and z is measured in centimeters in the axial direction from the throat of the stenosis. This results in a reduction in area (or %stenosis) of 84%. Axisymmetry was assumed around the longitudinal axis of the model geometry for numerical simulation. The time-averaged Navier-Stokes equations governing turbulent flow through the stenosis were solved using the FIDAP (Fluid Dynamics International, Evanston, IL, USA) CFD package. The FIDAP program uses a finite elements procedure, using the Galerkin form of the method of weighted residuals to solve the equations. In our model [steady incompressible turbulent flow in cylindrical coordinates z, r, and θ, assuming axisymmetry (*i.e.*, $v_\theta = \partial/\partial\theta = 0$)], the equations are:

$$\frac{1}{r}\frac{\partial}{\partial r}(r\overline{v_r}) + \frac{\partial \overline{v_z}}{\partial z} = 0 \qquad (2)$$

$$\rho\left(\overline{v_r}\frac{\partial \overline{v_z}}{\partial r} + \overline{v_z}\frac{\partial \overline{v_z}}{\partial z}\right) = -\frac{\partial \overline{p}}{\partial z} + \mu\left(\frac{1}{r}\frac{\partial}{\partial r}\left(r\frac{\partial \overline{v_z}}{\partial r}\right) + \frac{\partial^2 \overline{v_z}}{\partial z^2}\right)$$
$$ - \rho\frac{\partial}{\partial z}\overline{v_z'^2} - \frac{\rho}{r}\frac{\partial}{\partial r}\overline{rv_z'v_r'} \qquad (3)$$

$$\rho\left(\overline{v_r}\frac{\partial \overline{v_z}}{\partial r} + \overline{v_z}\frac{\partial \overline{v_r}}{\partial z}\right) = -\frac{\partial \overline{p}}{\partial r} + \mu\left(\frac{\partial}{\partial r}\frac{1}{r}\left(\frac{\partial}{\partial r}(r\overline{v_z})\right) + \frac{\partial^2 \overline{v_r}}{\partial z^2}\right)$$
$$ - \frac{\rho}{r}\frac{\partial}{\partial r}\overline{rv_r'} - \rho\frac{\partial}{\partial z}\overline{v_r'v_z'}, \qquad (4)$$

where $v_r = \overline{v_r} + v_r'$ and $v_z = \overline{v_z} + v_z'$ according to the Reynolds decomposition. The pressure is eliminated from the momentum equations (Eqs. 3 and 4) and solved from the continuity equation (Eq. 2) by replacing the zero on the right-hand side with a very small penalty parameter. Simulation of turbulent flow condi-

tions was applied by using the segregated solver method and the standard two equations $k - \varepsilon$ turbulence model, wherein the turbulent kinetic energy k and the viscous dissipation rate of turbulent kinetic energy ε are defined as follows:

$$k = -\overline{v_z'v_r'}; \qquad \varepsilon = v\,\overline{\left(\frac{\partial v_z'}{\partial r} + \frac{\partial v_r'}{\partial z}\right)^2}. \qquad (5)$$

In the standard two equation $k - \varepsilon$ turbulence model, typical eddy velocity and length scales (denoted by u_t and l_t) may be characterized as $\sqrt{k}$ and $k^{1.5}/\varepsilon$, respectively. An extension of this dimensional reasoning also leads to an expression for turbulent viscosity μ_t in terms of these characteristic scales of the turbulent eddies (*viz.* $\mu_t \propto \rho\,u_t\,l_t \propto \rho\,k^2/\varepsilon$). Thus μ_t is directly related to the turbulent quantities k and ε. Two transport equations for k and ε can then be obtained from the Navier-Stokes equations by a sequence of algebraic manipulations. In the vicinity of solid boundaries, the flow is dominated by viscosity, and the use of the $k - \varepsilon$ model may lead to inferior predictions. FIDAP uses specialized elements for near-wall modeling, in which the variation of the turbulent momentum diffusivity is modeled using van Driest's mixing length approach.

In the FIDAP program, the Galerkin finite element procedure is used to solve the Navier-Stokes equations. In general, a system of nonlinear algebraic equations that can be represented by the general matrix form $K(U) \times U = F$ can be solved, wherein K is a global system of matrices, U is the global vector of the unknowns [velocities, pressures, turbulent kinetic energy (k), and the viscous dissipation rate of turbulent kinetic energy (ε)], and F is the vector containing the boundary conditions, body forces, etc. The structure of the matrices depends on the nature of the specific problem being solved. Within each element, the dependent variables u_i and p are interpolated by functions of compatible order, in terms of values to be determined at a set of nodal points. In such element, the velocity and pressure fields are approximated by $u_i = \phi^T \mathbf{U}_i$, $p = \psi^T \mathbf{P}$, $k = \phi^T \mathbf{K}$, $\varepsilon = \phi^T \mathbf{E}$, wherein $\mathbf{U}_i$, $\mathbf{P}$, $\mathbf{K}$, and $\mathbf{E}$ are column vectors of element nodal point unknowns, and ϕ and ψ are column vectors of the interpolation functions. Substitution of these approximations into the field equations and application of the boundary conditions yield a set of equations, [*e.g.*, momentum: $f_1(\phi, \psi, \mathbf{U}_i, \mathbf{P}, \mathbf{K}, \text{and } \mathbf{E}) = \mathbf{R}_1$, etc.], where $\mathbf{R}_i$ are the residuals (errors) resulting from the use of the approximations. The Galerkin form of the method of weighted residuals seeks to reduce these errors to zero, in a weighted sense, by making the residuals orthogonal to the interpolation functions of each element (*i.e.*, ϕ and ψ).

FIGURE 2. Detail of the computational mesh in the area of the stenosis. The progressive density of the mesh in the radial direction shows the carefully modelled near wall region. A progressive mesh density in the axial direction was also applied to the inlet region, so that a plug flow velocity profile that evolved into a fully turbulent velocity profile could be applied as the inlet condition.

The progressive density of the finite elements mesh in the radial direction (Fig. 2; the stenosis area) shows the carefully modeled near-wall region. A progressive mesh density in the axial direction was also applied to the inlet region, so that a plug flow velocity profile that evolved into a fully turbulent velocity profile (where turbulence prevailed) could be applied as the inlet condition. A zero stress and zero pressure condition was applied at the outlet, and a no-slip condition was applied at the wall. The entrance length was conservatively chosen as 5 diameters so that the velocity profiles could be fully established proximal to the stenosis. To find the exit tube length, we examined wall stresses on the stenosis and the axial velocity profile in the center of the model. Results were independent of exit length for total model length >10 diameters. We conservatively selected a model length of 16.8 diameters (5 diameters entry length, 3.8 diameters stenosis section, and 8 diameters exit length). After establishing the numerical results to be independent of mesh density, the mesh consisted of 4,600 nine-node quadrilateral elements. In each element, biquadratic interpolation functions were used to approximate the velocities. The blood was assumed to be Newtonian, with real blood properties: $\rho = 1.056$ g/cm^3, $\mu = 3.5$ cP, and $\nu = 0.035$ cm^2/sec, so that accurate correlations may be made between the fluid simulations and actual blood platelet deposition determined from *in vitro* experiments.

Shear rate, $\dot{\gamma}$, was computed from the velocity gradient in the axial and radial directions, and elongational rate, $\dot{\xi}$, was computed from the velocity gradient in the axial direction (in axisymmetric cylindrical coordinates, r, z) as follows:

$$\text{shear rate: } \dot{\gamma} = \frac{\partial v_z}{\partial r} + \frac{\partial v_r}{\partial z}$$

$$\text{elongational rate: } \dot{\xi} = \frac{\partial v_z}{\partial z}. \tag{6}$$

The shear stress in the fluid (τ) was computed from

$$\tau_{rz} = \mu \left(\frac{\partial v_z}{\partial r} + \frac{\partial v_r}{\partial z} \right) - \rho \overline{v_z' v_r'}, \tag{7}$$

where ρ is the fluid density, and v_z' and v_r' are the turbulent velocity fluctuations in the axial and radial directions, correspondingly, wherever turbulence prevailed.

A platelet is exposed to varying levels of shear stress for varying durations as it passes through various flow regions; exceedingly high shear stresses at the contraction and throat regions of the stenosis for short exposure times, and a relatively high level of shear stress for a longer exposure time, when an individual platelet moves along the shear layer at the interface between the recirculation and core regions. Quantitative examination of the cumulative effect of these elevated shear histories would indicate whether platelets approaching the recirculation zone have a high incidence of activation. Therefore, time histories of individual platelets should be tracked down within the flow domain. Previous work (19) provided a crude estimation of the activation potential by computing the product of a bulk shear rate ($\dot{\gamma}$) and bulk average residence time assuming a Poiseuille flow in a tube. Hellums (11) depicted a platelet activation locus on a shear stress-exposure time domain, but results represent the action of constant shear stress levels with only the exposure time varying. No previous works known to these authors defined a platelet activation parameter that takes into account the cumulative effect of varying shear stresses and the time platelets exposed to them, let alone under turbulent flow conditions. With the detailed information that could be derived from our numerical simulations, the cumulative effect of shear stress and exposure time could be estimated by summing up the products of their instantaneous values along a streamline. Summation began at the inlet, Δt was the residence time of a platelet between two successive nodal points along a streamline, and $\bar{\tau}$ was the average shear stress value in that segment. This parameter was termed *level of activation*:

$$\sum \bar{\tau} \times \Delta t. \tag{8}$$

It must be cautioned that the cumulative effect of shear stress and exposure time on platelet trauma is probably nonlinear, so that the *level of activation* parameters can be regarded as an initial assessment of the process that may be refined by future studies.

To validate the numerical simulation, quantitative flow visualization was conducted using a digital particle image velocimetry (DPIV) system (Dantec FLOW-GRABBER, Dantec Measurement Technology, NJ, USA). The DPIV system is capable of providing a quantitative two-dimensional picture of displacement of particles and the velocity vector field of the flow. The fluid is seeded with particles and single exposure

images of the particles illuminated by a laser light sheet are recorded using a videocamera and a high-speed electronic shutter. Displacements of the particles are obtained by locally cross-correlating sequential images, and the velocity vector fields are computed from the known shutter speed. The cross-correlation function of the two samples is calculated using fast Fourier transform techniques. The displacement of the cross-correlation peak gives the average spatial shift of the particles in each subsample pair. To enhance the DPIV resolution, measurements were conducted in a steady flow loop with a large-scale stenosis model (10:1), following the previously described geometry. The model was manufactured from glass and had the following dimensions: inlet diameter, 9.9 cm; stenosis throat diameter, 3.96 cm; entry length of 25 diameters; and distal length of 16 diameters. The working fluid was water, seeded with reflective latex beads of 25 μm average diameter (Optimage Ltd., Edinburgh, UK) to obtain the velocity vector fields. Dynamic similarity was kept to run the DPIV measurements in the respective Re numbers (based on the upstream diameter) of the numerical simulations.

Previously measured platelet deposition results (20) were obtained by radioactive labeling of canine blood platelets with In-111, and quantified by measuring the percentage of radioactivity bound to platelets along successive segments of a model stenosis manufactured from transparent Lexan that was installed in a recirculating flow loop. The stenosis model had the same dimensions as the numerical model previously described. A steady flow peristaltic pump (Masterflex Model 7592) recirculated the blood through the flow loop, and a water bath (Buchi, Model 4061) maintained the blood temperature at 37°C. Platelets were labeled with In-111 tropolone using procedures described in detail by Dewanjee *et al.* (7) that routinely achieves a 90% platelet labeling efficiency. Results are given in terms of normalized platelet deposition (NPD), wherein the local number of platelets per unit area is normalized by the average platelet density along the entire test chamber.
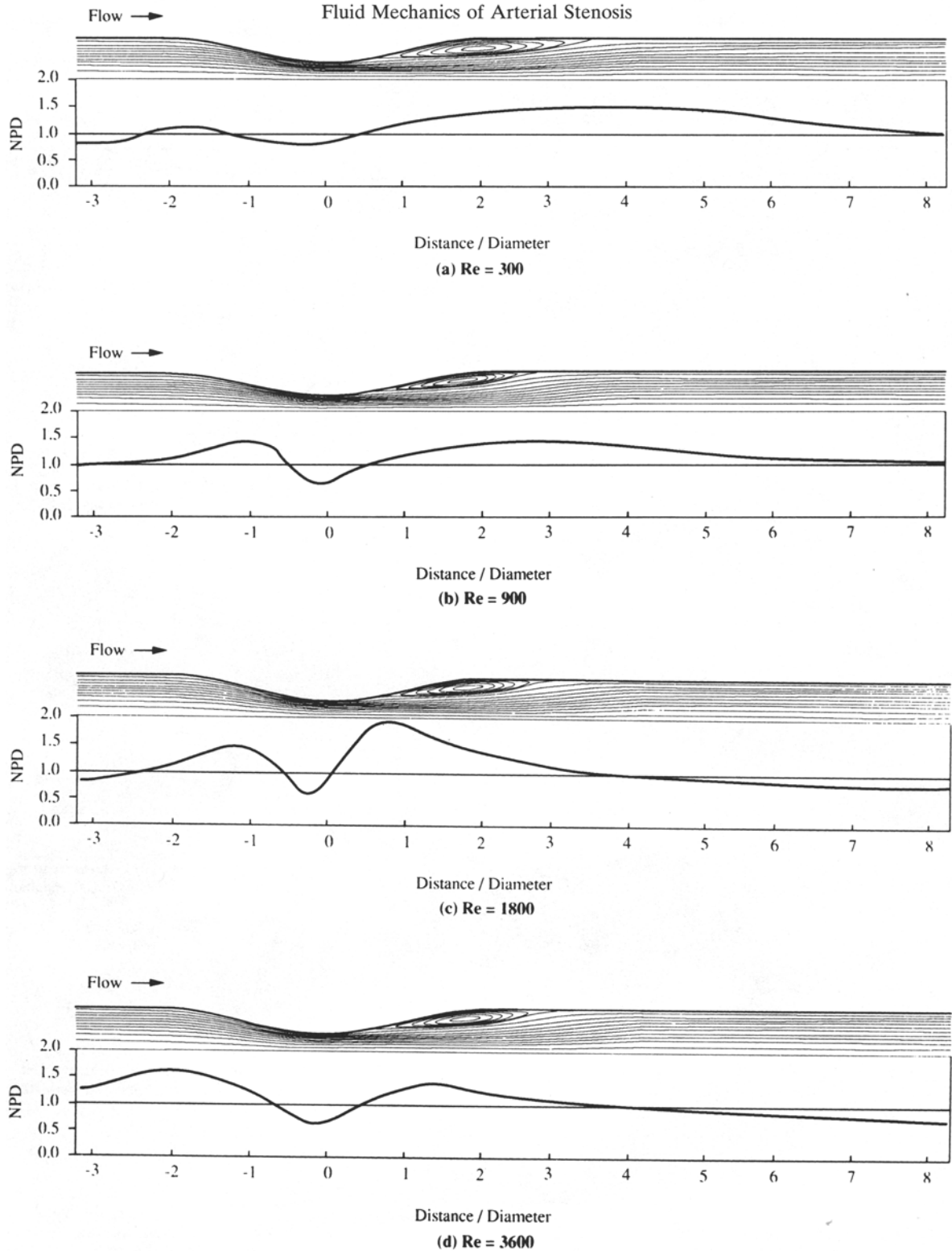
RESULTS

Numerical Results

Flow results were obtained at four different Reynolds numbers: Re = 300, 900, 1,800, and 3,600 (based on the proximal diameter and the average velocity at the inlet computed from the corresponding flow rates of 0.5, 1.5, 3, and 6 l/min). All results were characterized by a core jet flow pattern passing through the stenosis, surrounded by symmetrical recirculating vor-

tices in the expansion region (Fig. 3a–d). When flow conditions upstream were laminar (Re = 300, 900, and 1,800), the maximum core flow velocity through the stenosis was ~5 times larger than that of the tube inlet (Fig. 4a), indicating the strong acceleration of the central flow through the stenosis. Therefore, the main hemodynamic mechanism for platelet activation through the stenosis was the high shear stresses associated with the steep velocity gradient near the wall characteristic of jet flow, and the corresponding shear layer created between this jet and the slowly recirculating vortices distal the stenosis throat. The latter, characterized by low-wall shear stresses and long residence time of the trapped platelets, created the favorable conditions for the activated platelets to be deposited on the wall.

The streamline contour plots (Fig. 3a–d) show that, as the Reynolds number increased, the reattachment length decreased, thus reaching a minimum at Re = 1,800 and increasing slightly for Re = 3,600. This agrees with results by Young (25) in a flow through a sudden expansion. Young showed that the reattachment length in such flows increase with increasing Reynolds number for laminar flow conditions, peaks around Re = 300, and decreases with increasing Reynolds number, eventually reaching a limiting value at high Reynolds numbers. This behavior stems from the fact that the local Reynolds number at the throat is much higher than that of the upstream because of the strong convective acceleration. At Re = 300 (upstream), the local Reynolds number at the throat reaches a critical value in which the shear layer created between the jet and the surrounding fluid becomes unstable (26), thus affecting the size of the recirculation zone.

Experimental Validation of the Numerical Results with DPIV

Validation of the numerical simulation results was accomplished by comparing the numerical results to DPIV measurements conducted in a stenosis model with the same geometry in a steady flow loop. The numerical velocity profiles for Re = 300 (laminar case) were superimposed on a vector plot of the DPIV measurements (Fig. 4a). The superimposed dividing streamline of the recirculation zone according to the numerical simulation is in very good agreement with the DPIV results. Characteristic velocity profiles in the inlet, the stenosis throat, and the recirculation zone tightly overlap, with the measured DPIV velocity profiles somewhat lacking the finer resolution in the lower velocity range (the recirculation zone). For the turbulent case (Re = 3,600, Fig. 4b), a good agreement was

FIGURE 3. Streamlines and normalized platelet deposition (NPD) results for (a) Re = 300, (b) Re = 900, (c) Re = 1800, and (d) Re = 3600. Platelet deposition was measured previously using In-111 labeled platelets, and are shown here normalized by the average density of deposited platelets along the entire test chamber. Two distinct regions of increased platelet deposition were apparent, one proximal to and one distal to the stenosis throat. These areas of increased convective transport where locally curved streamlines contain velocity components perpendicular to the vessel wall. The size of the recirculation zone decreased in length at Re = 900 compared with Re = 300, with the center of the distal region of maximum NPD near the reattachment point in each case. For the higher Reynolds numbers, the highly disturbed turbulent jet strongly interacts with the separating flow, causing a distal increase in NPD nearer to the separation point.
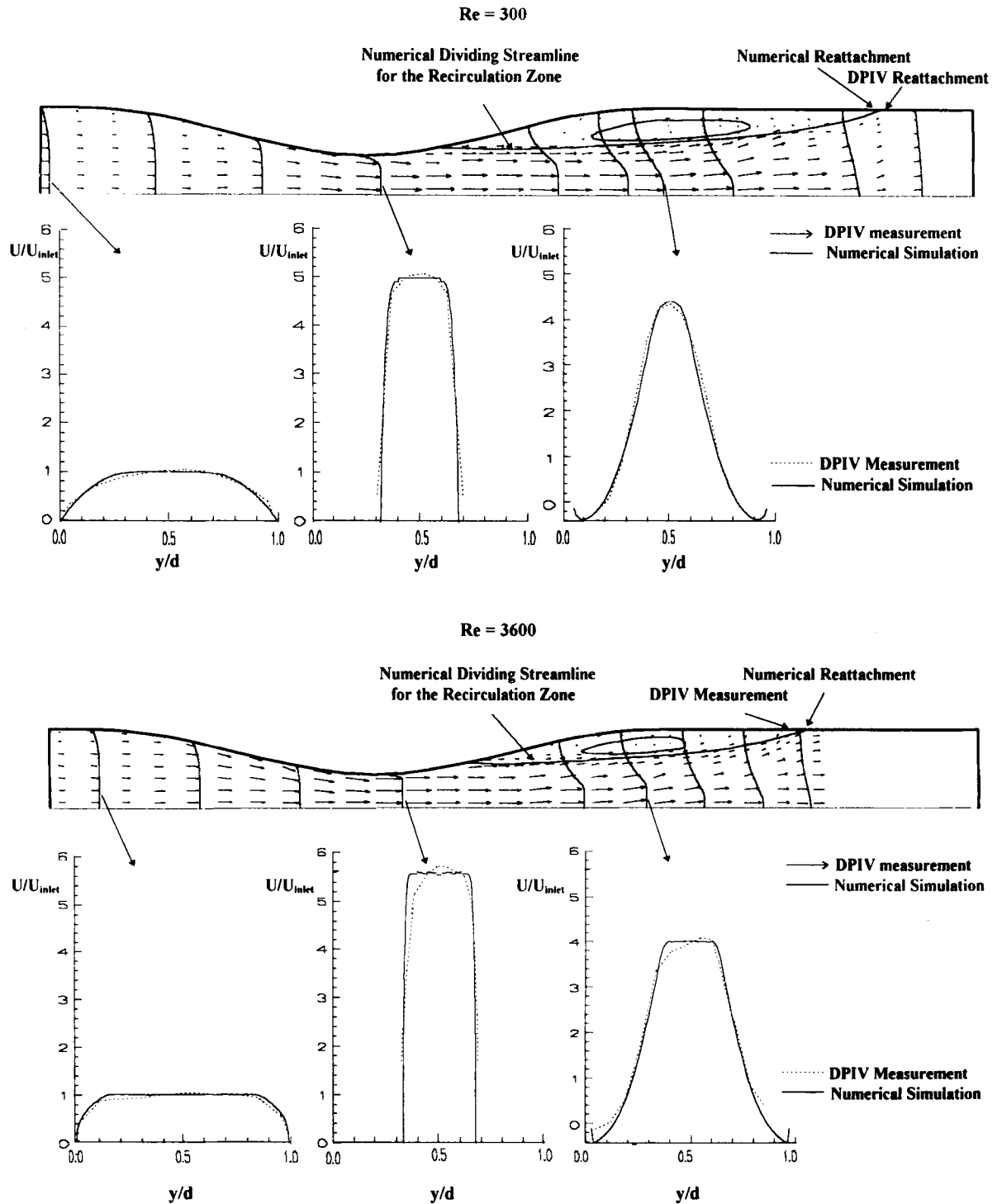
FIGURE 4. Comparison of Digital Particle Image Velocimetry (DPIV) measurements with numerical simulation results at (a) Re = 300 and (b) Re = 3600. The separation and reattachment points, denoted by the dividing streamline of the recirculation zone for the numerical simulation, are in very good agreement with the DPIV measurements for the laminar and turbulent cases. Characteristic velocity profiles tightly overlap, with the measured velocity profiles somewhat lacking the finer resolution in the lower velocity range (the recirculation zone).
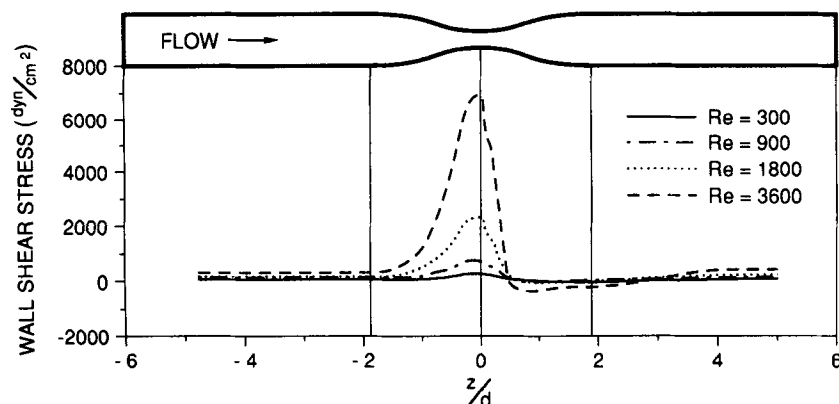
FIGURE 5. Wall shear stress distribution along the length of the stenosis model for the various simulations. While providing the opportunity for shear-induced platelet activation (see Fig. 7), the high shear stresses in the throat region also serve to wash away any potentially adherent platelets from the throat wall (see Fig. 3). The low shear stress along the wall in the recirculation region allow prolonged contact with the wall and thus a more suitable location for adhesion.

achieved between the numerical and DPIV results in predicting a characteristic fully turbulent velocity profile at the inlet, the stenosis throat, and in the recirculation zone. The prediction of the separation and reattachment points of the $k - \varepsilon$ turbulent model is in very good agreement with the DPIV results. This indicates that, although our numerical simulation of turbulent flow conditions was conducted at the low Re range, the combination of the $k - \varepsilon$ turbulent model with specialized elements for near-wall modeling, in which the variation of the turbulent momentum diffusivity is modeled using van Driest's mixing length approach, yielded a good prediction of the size of the recirculation zone and the turbulent mean velocities of the flow through the stenosis.

Shear Stresses and Exposure Time

Wall shear stress results are shown in Fig. 5. The wall shear stress rose sharply in the contraction region of the stenosis and peaked at the throat. The value of the wall shear stress peak was strongly dependent on the Reynolds number, indicating that transition to turbulence at the throat increases the wall shear stress by an order of magnitude. The wall shear stress declined rapidly to zero at the separation point ($z/d \approx -0.5$) and maintained a near-zero value (negative, because of the flow reversal in the recirculation zone) along the expansion region. As the separatory streamline leading to the point of reattachment ($z/d \approx 2.5$–3.5, depending on the Re number) defines the interface between the core flow and the recirculating flow, the shear layer created in this interface gradually increased the shear stress in the downstream direction until it approached the upstream value around $z/d = 4.5$.

The overall behavior of the shear rate within the flow domain is depicted in the three-dimensional surface plot (Fig. 6). The shear rate rises dramatically in the contraction region and peaks at the throat. Although shear rate drops sharply to near-zero negative

values inside the recirculation zone, a relatively high shear rate region, gradually decreasing in the downstream direction, is maintained in the shear layer between the core flow and the recirculation zone. The shear rate surface plot depicts this gradual decrease of this high shear region in a hillside fashion, descending into a valley-like region of negative shear in the recirculation zone.

The level of activation parameter ($\Sigma \bar{\tau} \times t$) of an individual platelet along a streamline is presented for Re = 3,600 (Fig. 7). A representative streamline that passes through regions of high shear stresses was chosen. The streamline passes near the wall in the upstream and the stenosis throat regions, and within the shear layer at the interface between the stenotic jet and the recirculation zone (Fig. 7). It is expected that most of the platelet activation due to elevated shear stresses will occur along these regions. The cumulative effect is shown in Fig. 7, compared with the shear history in a straight tube as extrapolated from events proximal to the stenosis. The comparison shows a step jump increase ($\sim 35\%$) in the level of activation parameter in the throat region. The elevated effect lasts throughout the recirculation zone until $z/D \approx 3.5$, and beyond, generally shifting the activation curve upward. As expected, platelets exposed to elevated shear stresses can be found in the vicinity of the recirculation zone.

Elongation stresses produced by the convective acceleration at the contraction zone toward the stenosis throat may also induce platelet activation. Elongation strain computed along the previously described streamline reached values of up to 600 sec^{-1} at Re = 3,600 (Fig. 8). Distal to the throat platelets experienced strong convective deceleration that produced negative elongation rates of $\sim 1,000$ sec^{-1}, indicating that the platelets experienced compression stresses immediately after their stretching. Adjacent to the recirculation zone ($z/D = 1$–3), the elongation rate alternated
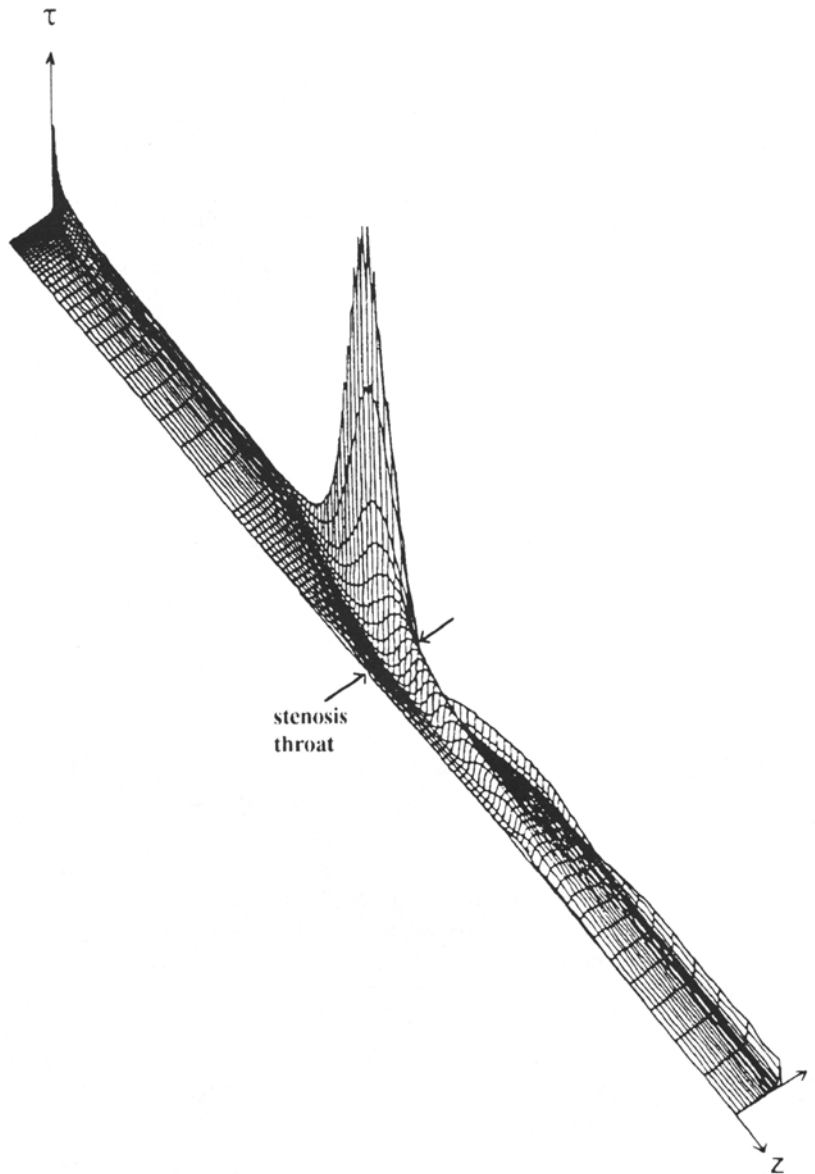
FIGURE 6. Perspective three dimensional view of the shear rate distribution within the flow domain. The high shear region near the wall at the throat extends downstream along the shear layer between the core flow and the recirculation zone, with a gradual decrease in the direction of flow. This provides favorable conditions for shear-induced platelet activation before subsequent entrapment in the recirculation zone.

between mild positive and negative values, finally stabilizing at mild positive elongation rates in the vicinity of the reattachment point ($z/D = 3$).

Correlation of Numerical Results with Blood Platelet Deposition Measurements

Results from the numerical simulations were correlated to previously published results (20) of experiments with canine blood flow (Fig. 3a–d). Platelet deposition was measured as a function of the axial position using In-111–labeled platelets and was normalized with respect to the average platelet deposition over the entire flow chamber. Increased platelet deposition was observed in areas of flow recirculation and

reattachment, with decreases in locations of high shear and separation. Two distinct regions of increased platelet deposition were apparent: one proximal to and one distal to the stenosis throat. At the lower Reynolds number (Re = 300, Fig. 3a), the recirculation zone extended to ~3.5 diameters downstream from the stenosis throat. The NPD curve peaked around the reattachment point and extended to ~7 diameters from the throat. At Re = 900 (Fig. 3b), the velocity profile at the throat indicated that the jet was becoming turbulent, thus inducing flow disturbances at the recirculation zone that was confined to ~2.8 diameters downstream. The distal region of increased NPD was likewise reduced in length, whereas the proximal NPD gained weight, coinciding with the increased contrac-
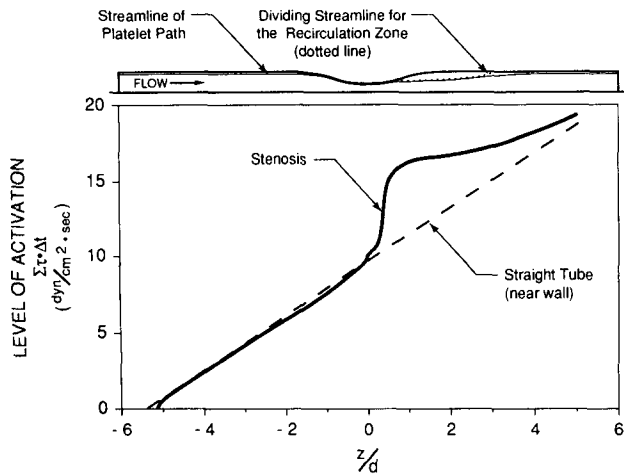
FIGURE 7. The value of the level of activation parameter (Eq. 8) for an individual platelet following a single streamline for the Re = 3600 simulation. The representative streamline chosen passes through regions of high shear near the wall and along the shear layer at the interface between the core jet and the recirculation zone. The cumulative effect of shear stress and exposure time displays the largest deviation from that of a straight tube under similar flow conditions in the region just past the stenosis throat. In this region the shear stresses are decreasing but still relatively high, and the flow is decelerating, allowing increased exposure time.

tion of the streamlines and the more vigorous acceleration. This trend continued for Re = 1,800 (Fig. 3c), with the NPD reaching a maximal value at the distal side of the stenosis. For Re = 3,600, the NPD peak at the proximal side of the stenosis was higher relative to that of the distal side. The upstream velocity profiles for Re = 3,600 (Fig. 3d) indicated that, for this Reyn-
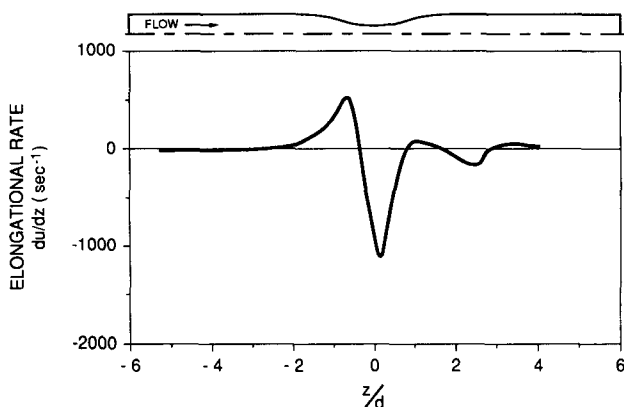
FIGURE 8. Elongation rate distribution along the identical streamline described in Fig. 7 for Re = 3600. Platelets traveling along this streamline experience stretching (positive elongation) just proximal to the stenosis throat and compression (negative elongation) just distal to the stenosis throat. These combinations of elongation stresses may also contribute to platelet activation prior to deposition in the downstream recirculation zone.

olds number, the upstream velocity was already fully turbulent.

DISCUSSION

In this model, local increases in shear stress and elongational stresses in the throat region were shown to increase the activation potential of the platelets. Immediately downstream of the stenosis, flow separating off the throat created a region of slowly recirculating flow conducive to aggregation of platelets and platelet-activating factors, creating a region of primary adhesion and subsequent aggregation of the activated platelets. Adhesion of platelets to a surface is greatly enhanced by prior activation. Platelet activation leads to loss of the disk shape of the resting platelet and the extrusion of pseudopods. Having undergone a shape change, the platelets continuously rotate in flow, covering with their pseudopods a hydrodynamically effective volume up to 8 times larger than in the inactivated state, which in turn increases the platelet-platelet collision frequency and with boundary (24). The contraction of the streamlines in the recirculation zone (Fig. 3a–3d) brings the platelets closer together, increasing the platelet-platelet collision frequency and with the boundary. The recirculation zone also enhances convective transport of platelets and blood cells to the vessel wall along locally curved streamlines (14,20).

This mechanism offers an explanation for the NPD distribution along the recirculation zone; platelets that are already activated by the high shear stresses at the throat and along the shear layer between the jet and the slowly recirculating vortices are brought into contact by the contracting streamlines on the slower side of this shear layer. Once trapped in the recirculation zone, the motion of the platelets along the curved streamlines with components perpendicular to the wall bring them into contact with the wall along the reattachment point and the slowly recirculating flow adjacent to the wall. For lower Reynolds numbers (Re = 300 and Re = 900), this mechanism causes the NPD distribution to reach a maximum around the reattachment point. The almost symmetric NPD distribution around it corresponds to streamlines leading platelets away from the wall in the counterclockwise direction (the proximal side of the recirculation zone) and the curved streamlines with velocity components perpendicular to the vessel wall beyond the point of reattachment (distal to the edge of the recirculation zone) that lead to a gradual decrease in the number of platelets deposited. The NPD peak at the proximal side of the stenosis is a result of the convective acceleration of the flow that is characterized by the contraction of the streamlines that increases the collision frequency

between the platelets. Although acting as a platelet activation agent, the high shear stress at the wall of the throat itself washes away the platelets, preventing their adhesion to the wall.

At Re = 900, the velocity profiles indicate that the jet produced by the stenosis is turbulent and continues to be so in the expansion region. At Re = 1,800, this trend is exacerbated. The NPD curve peaks in the vicinity of the separation point, indicating that the highly disturbed jet strongly interacts with the separating flow, increasing the platelet collision rate and adhesion to the wall at this location. As turbulence intensifies, activating more platelets and increasing even more the collision rate, a pronounced NPD peak is produced at the distal side of the stenosis. At Re = 3,600, the upstream velocity profiles indicate that the flow is already fully turbulent. The increased collision rate characteristic of fully turbulent flow conditions, coupled with the contracting streamlines toward the throat, increases the platelet deposition at the proximal side of the throat relative to the decreasing number of platelets in the distal region, thus producing a higher NPD peak at the proximal side of the stenosis.

The wall shear stress distribution along the stenosis offers further insight to the NPD curves behavior. Although high wall shear stresses activate the platelets at the contraction region, the high wall shear stress at the throat tends to wash away platelets from the throat. This explains the minimum NPD value at the throat, characteristic of the NPD curves for all Reynolds numbers. The activated platelets that are then trapped in the recirculation zone experience very low wall shear stresses, allowing prolonged contact with the wall. This phenomenon confirms theoretical predictions by Basmadjian (3) and others that increased platelet deposition on an artificial surface depends on the ability of the local geometry to enhance transport of platelets to the vessel wall, as well as a diminished capacity to embolize these deposits through decreased wall shear stresses. With intensifying turbulence, turbulent wall shear stresses are around one order of magnitude larger than for the laminar cases. Even at relatively low Reynolds numbers, wherein the upstream flow conditions are laminar, our numerical simulations clearly show that parts of the flow field, namely the stenotic jet, can become turbulent. Thus, it is important to conduct numerical simulations using turbulence modeling at subcritical Reynolds numbers of the corresponding pipe flow conditions.

Platelets are exposed to high shear stresses at the contraction and throat regions of the stenosis for relatively short exposure time due to the flow acceleration in these regions. After that, an individual platelet that flows along the shear layer at the interface between the recirculation and core regions is still exposed to a relatively high level of shear stress, for a longer exposure time, due to the slowing velocities at the expansion region. When one examines the cumulative effect of these elevated shear histories, there is a clear indication that platelets approaching the recirculation zone have high incidence of activation. The level of activation parameter (Fig. 7) shows this effect as a steep increase in the level of activation parameter at the throat region that lasts throughout the recirculation zone, shifting the activation curve upward. Although after the recirculation zone, the activation curve returns to a value only slightly higher than that of a straight tube, the higher incidence of activation lasts throughout the recirculation zone, wherein most of the platelets are deposited according to the NPD curves (Fig. 3a–d).

Despite the relatively high values of the activation parameter, these values were below those required for platelet activation under steady flow conditions. Ramstack et al. (19) measured platelet activation induced by short-time exposure to high shear stress in small tubes. They found that under constant shear rate, procoagulant platelet factor 3 (FP3) is released above $\{\dot{\gamma} - \text{shear rate}\} \times \{t - \text{exposure time}\} = 10^3$. In our analysis of the platelet activation factor, for Re = 3,600 at the recirculation zone, $\Sigma\bar{\tau} \times t \approx 17$ (dyne $\times$ sec/cm^2). Multiplying the parameter of Ramstack *et al.* by $\mu_{\text{blood}} = 0.035$ g/cm-sec to obtain the parameter in our platelet activation factor units, we get $\Sigma\bar{\tau} \times t = 35$ (dyne $\times$ sec/cm^2), twice the value of our parameter. Given the evidence that unsteady shear enhances platelet activation, compared with constant shear (22), and the effect of the additional turbulent stresses in our experiment (compared with Ramstack *et al.*'s laminar flow conditions), it may be speculated that platelet activation is already reached at $\Sigma\bar{\tau} \times t \approx 17$, so that activation might occur even during a single passage of the platelet through the stenosis at these flow conditions (Re = 3,600).

The levels of shear stresses used in our study, their variation, and their duration approximate that found in the human cardiovascular system. Most previous work was conducted in steady flow devices that produced constant shear stresses, in most cases for durations that were orders of magnitude longer than physiological. In our closed experimental loop for platelet deposition measurement, platelets experienced repeated passages through the stenosis. The loop consisted of a tube ~2.5 ft long, resulting in the platelet passing through the stenosis approximately every 1 to 2 sec. Moreover, in our experiment, other factors (*i.e.*, pump action, radioactive labeling procedure, contact with foreign surfaces, and use of whole blood in which

red blood cells may potentiate platelet activation via adenosine diphosphate release once a certain degree of shear stress is reached) may induced further activation. Thus, it may be realistic to assume that, in our flow loop, once activated, platelets remained that way throughout the experiment.

When an individual platelet flows through the contraction and the expansion of the stenosis, it also experiences elongational stresses. Our computations show that the platelets first experience a considerable amount of stretching through the contraction, followed by a strong compression stress through the expansion of the stenosis (Fig. 8). There is experimental evidence to support the postulate that stretching of platelet membranes enhances platelet activation through increased ion permeability and increased receptivity to ligand binding (18). The combined effect of stretching followed by compression and alternation between the two, as found by our analysis, has not been studied yet in terms of platelet activation. The elongational stresses occur at locations that partially overlap the elevated shear stresses regions; therefore, it seems plausible that these stresses contribute to platelet activation and may correspond to activation at lower levels of shear stresses found in our model, compared with that found in constant shear devices, such as cone and plate viscometers. Such experimental evidence would be instrumental in formulating a more prudent activation parameter that incorporates all pertaining stresses experienced by a platelet.

CONCLUSIONS

In this study, direct qualitative and quantitative correlations of fluid dynamic parameters with platelet deposition onto artificial surfaces were obtained. The stenosis geometry produced localized regions of high and low shear, flow separation, recirculation, and reattachment, thus enhancing transport of platelets and clotting factors to the vessel wall along contracted and locally curved streamlines with velocity components perpendicular to the vessel wall. Activation potential of platelets was enhanced in regions where the platelets were exposed to high shear stresses. As the Reynolds number increased, the shear layer between the stenotic jet and the recirculation zone became unstable, intensifying turbulence and consequently increasing the shear stresses within the flow domain, as well as the wall shear stresses. The cumulative effect of these stresses and the time the platelets were exposed to them was obtained (the level of activation parameter), indicating that platelets approaching the recirculation zone had a high incidence of activation. It was also shown that, whereas the platelets flow through the regions of elevated shear stresses, they experience elongational stresses of stretching and compression that may contribute to their level of activation. Once activated, actual platelet deposition onto the wall was dependent on the wall shear stress level. Although embolization forces were high at the throat, where the wall shear stress peaked, the decreased wall shear stress in the recirculation zone diminished the capacity of the geometry to embolize the deposits and at the same time allowed prolonged contact with the wall. Whereas our numerical simulations clearly indicate that the stenosis geometry enhanced the platelet activation potential, due to our closed loop experimental arrangement the platelets experienced repeated frequent passages through the stenosis that possibly activated them prior to an individual passage through the stenosis. This may explain the increased platelet deposition evident in our NPD curves, even though the level of activation parameter, when compared with other researchers' results, did not indicate that activation was actually reached. Nevertheless, it is clear that studying the cumulative effects of the various stresses that platelets experience along their path lends to a more realistic depiction of the platelet activation process under physiological conditions.

The current study was conducted under steady flow conditions. However, under physiological conditions, platelets not only experience varying shear stresses for varying durations when flowing through a stenotic artery, but also the effects of flow pulsatility. Transient effects of the flow pulsatility must be studied as well. Also, more studies of the biochemical cascade leading to platelet activation under more realistic conditions are needed, so that data are available to correlate with results of fluid dynamic studies through stenosed vessels like the current one. These studies should include the cumulative effects of platelet activation history in terms of varying shear stresses that correspond to physiological time scales and the effects of elongational stresses (stretching and compression) on the activation process.

REFERENCES

1. Aarts, P. A., M. M. van Den, S. A. T. Broek, G. W. Prins, D. C. Kuiken, J. J. Sixma, and R. M. Heethaar. Blood platelets are concentrated near the wall and red blood cells, in the center in flowing blood. *Arteriosclerosis* 8:819–824, 1988.
2. Badimon, L., and J. J. Badimon. Mechanisms of arterial thrombosis in nonparallel streamlines: platelet thrombi grow on the apex of stenotic severely injured vessel wall. *J. Clin. Invest.* 84:1134–1144, 1989.
3. Basmadjian, D. The effect of flow and mass transport in thrombogenesis. *Ann. Biomed. Eng.* 18:685–709, 1990.

4. Christenson, J. T., J. Mergerman, K. C. Hanel, G. J. L'Italien, H. W. Strauss, and W. M. Abbott. The effect of blood flow rates on platelet deposition in PTFE arterial bypass grafts. *Trans. ASAIO J.* 27:188–191, 1981.

5. Colantuoni, G., J. D. Hellums, J. L. Moake, and C. P. Alfrey, Jr. Response of human platelets to shear stress at short exposure times. *Trans. Am. Soc. Artif. Organs* 23:626–630, 1977.

6. Deshpande, M. D., and D. P. Giddens. Computation of turbulent flow through constrictions. *Eng. Mech.* 109:466–471, 1983.

7. Dewanjee, M. K., M. Kapadvanjwala, W.-W. Mao, W. Jy, Y. Ahn, K. Ruzius, A. K. Ghafouripour, A. N. Serafini, and G. N. Sfakianakis. A higher blood flow window of reduced thrombogenicity and acceptable fragmentation in a hollow fiber hemodialyzer. *ASAIO J.* 39:M363–M367, 1993.

8. Eckstein, E. C., and F. Belgacem. Model of platelet transport in flowing blood with drift and diffusion terms. *Biophys. J.* 60:53–69, 1991.

9. Eldrup-Jorgensen, J., W. C. Mckey, and R. J. Connoly. Evaluation of arterial prosthesis in a baboon ex vivo shunt: the effect of graft material and flow on platelet deposition. *Am. J. Surg.* 150:185–190, 1985.

10. Folie, B. J., and L. V. McIntire. Mathematical analysis of mural thrombogenesis: concentration profiles of platelet-activating agents and effects of viscous shear flow. *Biophys. J.* 56:1121–1141, 1989.

11. Hellums, J. D. Biorheology in thrombosis research. *Ann. Biomed. Eng.* 22:445–455, 1994.

12. Hellums, J. D., D. M. Peterson, N. A. Stathopoulos, J. L. Moake, and T. D. Giorgio. Studies on the mechanisms of shear-induced platelet activation. In: Cerebral ischemia and hemorheology, edited by A. Hartman and W. Kuschinsky. New York: Springer-Verlag, 1987, pp. 80–89.

13. Karino, T., and H. L. Goldsmith. Aggregation of human platelets in an annular vortex distal to a tubular expansion. *Microvasc. Res.* 17:217–237, 1979

14. Karino, T., and H. L. Goldsmith. Adhesion of human platelets to collagen on the walls distal to a tubular expansion. *Microvasc. Res.* 17:238–262, 1979.

15. Karino, T., H. L. Goldsmith, M. Motomiya, S. Mabuchi, and Y. Sohara. Flow patterns in vessels of simple and complex geometries. In: Blood in contact with natural and artificial surfaces, edited by E. F. Leonard, V. T. Turitto, and L. Vroman. New York: New York Academy of Sciences, 1987, pp. 422–441.

16. Lassila R., J. J. Badimon, S. Vallabhajosula, and L. Badimon. Dynamic monitoring of platelet deposition on severely damaged vessel wall in flowing blood. *Arteriosclerosis* 10:306–315, 1990.

17. Lelah, M. D., L. K. Lamprecht, and S. L. Cooper. A canine ex vivo series shunt for evaluating thrombus deposition on polymer surfaces. *J. Biomed. Mater. Res.* 18:475–496, 1984.

18. Purvis, N. B., and T. D. Giorgio. The effects of elongational stress exposure on the activation and aggregation of blood platelets. *Biorheology* 28:355–367, 1991.

19. Ramstack, J. M., L. Zuckerman, and L. F. Mockros. Shear induced activation of platelets. *J. Biomech.* 12:113–125, 1979.

20. Schoephoerster, R. T., F. Oynes, H. Nunez, M. Kapadvanjwala, and M. K. Dewanjee. Effects of local geometry and fluid dynamics on regional platelet deposition on artificial surfaces. *Atheroscler. Thromb.* 12:1806–1813, 1993.

21. Stein, P. D., and H. N. Sabbah. Measured turbulence and its effect on thrombus formation. *Circ. Res.* 35:608–614, 1974.

22. Sutera, S. P., M. D. Nowak, J. H. Joist, D. J. Zeffren, and J. E. Bauman. A programmable, computer-controlled, cone-plate viscometer for the application of pulsatile shear stress to platelet suspensions. *Biorheology* 25:449–459, 1988.

23. Tangelder, G. J., D. W. Slaaf, H. C. Teirlink, R. Alewijnse, and R. S. Reneman. Localization within a thin optical section of fluorescent blood platelets flowing in a microvessel. *Microvasc. Res.* 23:214–230, 1982.

24. Wurzinger, L. J., P. Blasberg, and H. Schmid-Schönbein. Towards a concept of thrombosis in accelerated flow: rheology, fluid dynamics, and biochemistry. *Biorheology* 22:437–449, 1985.

25. Young, D. F. Fluid mechanics of arterial stenosis. *J. Biomech. Eng.* 101:157–175, 1979.

26. Young, D. F., and F. Y. Tsai. Flow characteristics in models of arterial stenosis. I. Steady flow. *J. Biomech.* 76:395–410, 1973.